JOURNAL OF THE MECHANICAL BEHAVIOR OF BIOMEDICAL MATERIALS 31 (2014) 68–76

Available online at www.sciencedirect.com

ScienceDirect

www.elsevier.com/locate/jmbbm

Research Paper

In situ measurements of local temperature and contact stress magnitude during wear of ceramic-on-ceramic hip joints

Wenliang Zhu[a], *Leonardo Puppulin*[b], *Andrea Leto*[c], *Yasuhito Takahashi*[b], *Nobuhiko Sugano*[a], *Giuseppe Pezzotti*[b,d,*]

[a]*Department of Orthopedic Surgery, Osaka University Medical School, 2-2 Yamadaoka, Suita, 565-0871 Osaka, Japan*
[b]*Ceramic Physics Laboratory and Research Institute for Nanoscience, Kyoto Institute of Technology, Sakyo-ku, Matsugasaki, 606-8585 Kyoto, Japan*
[c]*Piezotech Japan Ltd., Mukaibata-cho 4, Ichijoji, Sakyo-ku, 606-8326 Kyoto, Japan*
[d]*The Center for Advanced Medical Engineering and Informatics, Osaka University, 2-2 Yamadaoka, Suita, 565-0817 Osaka*

ARTICLE INFO

Article history:
Received 27 July 2012
Received in revised form
9 January 2013
Accepted 25 January 2013
Available online 9 February 2013

Keywords:
Fluorescence spectroscopy
Tribometer
Ceramic hip joints
Contact stress
In situ temperature analysis

ABSTRACT

Fluorescence microprobe spectroscopy was applied to *in situ* assessments of contact stress and local temperature at the contact point of dry-sliding couples during wear tests of two commercially available ceramic-on-ceramic femoral heads. The investigated ceramic hip implants consisted of either monolithic Al_2O_3 or Al_2O_3/ZrO_2 composite. A specially designed pin-on-ball tribometer was employed, which enabled directly testing the femoral head components as received from the maker without further manipulation. The strong fluorescence emission from Cr^{3+} impurities contained in Al_2O_3 served as a responsive sensor for both temperature and stress. Analytical corrections for the averaging effects arising from the finite size of the laser probe were made according to a probe response formalism in which geometrical conditions of the sliding couple were incorporated as boundary conditions. The sample-probe interaction at the contact point was then experimentally calibrated by obtaining probe response functions for the two materials investigated. Based on such theoretical and experimental procedures, deconvolutive computational routines could be set up and the true variations of local temperature and stress at the contact point of the bearing surfaces retrieved from the observed time-dependent broadening and shift of a selected spectral band, respectively. The main result of the *in situ* investigation was that the monolithic sliding couple showed both significantly lower temperature and lower magnitude of compressive stress at the contact point as compared to the composite one, although the composite couple wore at a significantly lower specific wear rate than the monolithic one.

*Corresponding author at: Ceramic Physics Laboratory and Research Institute for Nanoscience, Kyoto Institute of Technology, Sakyo-ku, Matsugasaki, 606-8585 Kyoto, Japan. Tel./fax: +81 75 724 7568.
E-mail address: pezzotti@kit.ac.jp (G. Pezzotti).

1751-6161/$ - see front matter © 2013 Elsevier Ltd. All rights reserved.
http://dx.doi.org/10.1016/j.jmbbm.2013.01.018

1. Introduction

In vitro wear testing according to various tribological methods has been long and widely applied to the characterization of frictional forces and wear rates in load-bearing materials (Nair et al., 2009; Korres and Dienwiebel, 2010; Zemzemi et al., 2008; Patton and Zabinski, 2002; Kerkwijk et al., 1999; Cherif et al., 1997), as well as directly on hip joints by means of hip simulators (Saikko, 2005; Goldsmith and Dowson, 1999; McKellop and D'Lima, 2008; Ramamurti et al., 1998). Such approach not only enables estimating the wear resistance of the sliding materials but also provides important hints about the expected *in vivo* longevity of the implant. Nowadays, various kinds of tribometer device are available, which are routinely used to characterize the tribological properties of materials used in a variety of technologies. Among the available devices, the most basic equipments involve a flat or spherical surface that is driven by an external weight to move repetitively across the face of the tested material. The latter case corresponds to the classic pin-on-disc frictional test, as applied by Kerkwijk et al. (1999) for the evaluation of friction and wear characteristics of alumina and zirconia ceramics.

During wear testing, the occurrence of contact stress and the generation of heat at the contact area is inevitable. The sliding contact might cause quite severe temperature/stress gradients in the vicinity of the contact point (or surface) and represents the origin of structural degradation at the material surface. In current tribological assessments, precise but conspicuously phenomenological comparisons of the overall damage resistance can be made among different materials, but the physical, chemical and mechanical states of the material surface at the contact point are usually not explicitly represented in the monitored parameters. Some attempts have indeed been made to improve this situation. In the field of ceramic materials, Cherif et al. (1997) investigated the wear behavior of alumina–zirconia composites and measured the temperature in the mid-thickness of the disk sample during tribological test using a K-type thermocouple, which was fixed by means of alumina cement in a hole drilled in the disk. Unfortunately, this method was far from leading to accurate results, as far as the actual temperature value at the contact point between sliding surfaces was the target of the investigation. Nevertheless, this *in situ* attempt was conceptually important because it emphasized the possibility of expanding the outputs of conventional wear measurements from a merely phenomenological to a more physically insightful level. In the specific context of this paper, we notice that an improved *in situ* approach could play a quite relevant role in tribological testing of ceramic-on-ceramic bearing biomaterials, the most recent protagonists in the new generation of low-friction materials for arthroplastic applications (Piconi et al., 2003). However, for unfolding the local state of the material *in situ* at the contact point in such an important class of advanced materials, screening with high spatial resolution is needed. Therefore, a quite focused and responsive sensing mechanism is required. Succeeding in such a difficult task would contribute to comprehensively unveil not only the dynamics but also the inherent physics of the complex ensemble of wear phenomena.

Photo-stimulated spectroscopy can be regarded as a viable and quite powerful tool for realizing advanced tribological assessments. Shift and broadening of photo-stimulated spectral bands can bring direct and quantitative information about local temperature and stress fields, and other microstructural features occurring during wear of ceramic biomaterials such as alumina and zirconia. *In situ* tribological tests combined with fluorescence microprobe spectroscopy have a potential for fully satisfying all the requirements for an effective evaluation of the wear phenomena occurring at the contact point. However, as far as the geometry of a pin-on-disk tribometer is concerned, a direct application of photo-stimulated spectroscopy with the tribometer being placed under the optical microscope for *in situ* investigations could be problematic. In order to focus the laser at the contact point between the sliding surfaces, the pin (or the disk) should be made of a transparent material (e.g., glass or sapphire (Joly-Pottuz et al., 2007)). By doing so, however, the characteristics of the sliding couple become altered to a large extent, and thus the obtained tribological results cannot directly reflect the wear behavior of the actual sliding couple under evaluation. In other words, a different approach is needed for practical *in situ* studies of wear damage in biomedical sliding couples.

In this paper, we present *in situ* assessments of contact stress and local temperature at the contact point (or area) during sliding wear of ceramic-on-ceramic hip joints, as obtained in a specifically designed pin-on-ball tribometer by means of fluorescence microprobe spectroscopy. Leaving aside the full details of the new tribometer equipment, which are extensively given in a companion paper (Puppulin et al., in press), here, two different ceramic-on-ceramic hip couples (i.e., monolithic alumina and alumina/zirconia composite) widely used for hip joint replacements are investigated and compared in order to demonstrate the feasibility of this newly proposed spectroscopy-assisted tribology test. The selected sliding geometry and the use of a long-focus objective lens enables focusing, through precise calibrations, the incoming laser exactly at the contact point, while collecting the excited spectral signals from a relatively narrow probe volume. However, a serious complication arises from broadening of the fluorescence probe below the contact point from both sides of the sliding counterfaces. In order to solve this problem, the sample-probe interaction at the contact point was systematically analyzed from both theoretical and experimental viewpoints, and algorithms given to quantitatively describe a probe response function for the two studied sliding couples. Accordingly, probe averaging effects in space were removed through deconvolutive computational routines, and the true variation of local temperature and stress at the contact point retrieved within a degree of precision from the time-dependent broadening and shift of selected spectral bands.

2. Experimental procedures

2.1. Pin-on-ball tribometer for in situ photo-stimulated spectroscopy

Fig. 1 schematically shows the geometry of the specially designed tribometer, which enables wear tests with concurrent *in situ* investigations by fluorescence spectroscopy. A full description of the tribometer is given in a companion paper (Puppulin et al., in press). Briefly, the tribometer consists of a fixed pin and

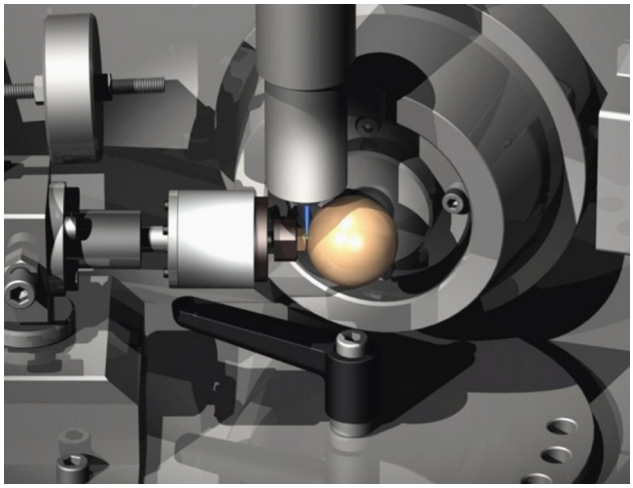

Fig. 1 – Geometry of the specially designed pin-on-ball tribometer placed under the objective lens of a Raman microprobe spectrophotometer.

a rotating femoral head, brought into contact by an externally applied controlled load. The all tribometer device is placed under an optical microscope equipped with a long-focal-length objective lens, which enables focusing the laser beam at the contact point between the pin and the femoral head, while also collecting the fluorescence backscattered signal *in situ* emitted during tribological tests.

Fluorescence spectroscopic experiments were carried out in a backscattering configuration with using a triple monochromator (T-64000, Horiba/Jobin-Yvon, Kyoto, Japan) equipped with liquid nitrogen-cooled charge coupled device (CCD). The 514 nm line of an Ar-ion laser (Stabilite 2017, Spectra-Physics, Mountain View, CA) was employed as an excitation source with a maximum power of 300 mW. Experiments were conducted in a confocal probe configuration with the pinhole aperture of the optical circuit set to 100 μm. Spectral lines were analyzed with the aid of a commercially available software package (Labspec 4.02, Horiba/Jobin-Yvon, Kyoto, Japan). Fitting was performed according to Gaussian–Lorentzian spectral modes after subtracting a linear baseline. The mathematical procedures followed for the theoretical calculations were carried out with the aid of commercially available computational software (Mathematica 5.2; Wolfram Research Inc., Champaign, IL).

2.2. *Wear testing*

Wear conditions were set according to the international standards (ASTM G99/G95, DIN 50324 and ISO/FDIS 20808:2003(E)), which give guidance for conducting wear tests in a ball-on-disc configuration. After pin and femoral head were mounted into their holders, the eccentricity of the rotating ball was carefully adjusted with using a profilometer stylus until it could be systematically confined to $<10\,\mu m$. The non-rotating pin slid along the maximum diameter of the rotating femoral head with the axes of pin and head forming a contact angle of 45°. A constant load of 10 N was applied by a lever-arm device and the sliding velocity was set at a constant value, $V=0.1$ m/s. During sliding, the magnitude of forces parallel and perpendicular to the sliding surfaces at the contact point was monitored (together with the concurrent acquisition of fluorescence spectra) as a function of sliding distance. An initial period of about 0.5 h elapsed until the wear parameters reached stable values. All tribological tests were run under dry conditions and were intentionally interrupted when the sliding distance reached 2×10^3 m.

2.3. *Hip-joint ceramic samples*

The investigated implants included two kinds of commercially available ceramic biomaterial for artificial hip joints: BIOLOX®*delta* and BIOLOX®*forte* (both manufactured by CeramTec, Plochingen, Germany). BIOLOX®*delta* is a composite material consisting (after sintering) of 80 vol% Al_2O_3, 17 vol% ZrO_2, and 3 vol% strontium aluminate. Y_2O_3 and Cr_2O_3 were added to the raw materials in quantities of 0.6 wt% and 0.3 wt%, respectively, together with a minor fraction of SrO. After sintering, Y and Cr elements were found mainly solved in the grain structure. No porosity could be observed in the microstructural arrangement. The sizes of alumina and zirconia grains were typically in the order of 1.0 μm and 0.3 μm, respectively. A small fraction of platelet-shaped grains, consisting of strontium hexaluminate, was dispersed in the microstructural network. The apparent aspect ratio of the platelets in the plane of polish was typically between 3 and 6. The BIOLOX®*forte* material was made of monolithic polycrystalline alumina. Its impurity contents were: $(SiO_2+CaO+Na_2O)<0.05$ wt% and $MgO<0.25$ wt%. The average size of the alumina grains was 1.4 μm. Composite and monolithic biomaterials will be henceforth simply referred to as *delta* and *forte*, respectively. All the analyzed femoral heads were 28 mm in diameter, and were self-worn against pins with the same surface curvature as the tested head, which were obtained from cutting separate femoral heads made of the same material.

3. Theoretical assessments

3.1. *Probe response function for the sliding couple*

In a microprobe spectroscopic device, when the laser beam is focused at an arbitrary location $P_0\equiv(x_0,y_0,z_0)$ on the sample, the intensity of the observed fluorescence spectrum, $I_{obs}(\omega)$, is convoluted within the volume of the probe and arises from a plethora of individual spectra scattered from individual locations, $P\equiv(x,y,z)$, comprised within the probe volume. Individual intensity contributions to the emitted signal are weight-averaged through a probe response function (PRF), namely, the morphological function characterizing the laser probe geometry when it interacts with the sample. The PRF, $G(x,x_0,y,y_0,z,z_0)$, depends on the location of the impinging laser, $P_0(x_0,y_0,z_0)$, and that of the scattered light, $P(x,y,z)$, and can be described as follows (Lipkin and Clarke, 1995; Atkinson and Jain, 1999; Zhu and Pezzotti, 2005):

$$I_{obs}(x_0,y_0,z_0)\propto\iiint_V I(\omega)G(x,x_0,y,y_0,z,z_0)dxdydz=\iiint_V\frac{A^2}{(\omega-\omega_p)^2+A^2}$$

$$\times\left\{\Omega_{xyz}\frac{p^2}{p^2+(z-z_0)^2}e^{-2\alpha_{eff}Z_a(x,y)}e^{\left[-2\frac{(x-x_0)^2+(y-y_0)^2}{B(z)^2}\right]}\right\}dxdydz \quad (1)$$

where $I(\omega)$ is the local spectral line shape, with peak width, $2A$, and peak position, ω_p, p a constant referred to as the probe response parameter, α_{eff} the effective absorption coefficient of the material at the incident wavelength, Z_a the effective depth of absorption, and V the probe volume. $B(z)$ is the laser beam width in planes perpendicular to the axis of the incoming laser. It depends on both the numerical aperture, NA, of the objective and the refractive index, n, of the material, as follows:

$$B(z)=\sqrt{B_0^2+\left\{z\tan\left[\arcsin\left(\frac{NA}{n}\right)\right]\right\}^2} \quad (2)$$

B_0 is a constant and the function, Ω_{xyz}, is defined as the collection solid angle at a given spatial position, being related to both the focal length, f, and the diameter, D, of the objective lens, as:

$$\Omega_{xyz}\approx 2\pi\left[1-\frac{f+z}{\sqrt{(f+z)^2+\left(\frac{D}{2}\right)^2}}\right] \quad (3)$$

Fig. 2(a) shows the configuration of both Cartesian and spherical coordinate systems, as selected in this study for describing the probe sample interaction in the pin-on-ball tribometer. When the laser beam is focused at an arbitrary position on the surface of the ball, the configuration of the sample-probe system and the selection of the coordinate systems on the ball can be represented as shown in Fig. 2(b). With neglecting refraction, the light scattered from any arbitrary position $P(x,y,z)$ inside the fluorescence probe and reaching the objective lens should pass through the surface of the ball at Q before reaching the objective lens. According to simple geometrical considerations on the drafts of Fig. 2, the following equations can be obtained:

$$\frac{|\overline{QM}|}{f+z}=\frac{Z_a}{\sqrt{(f+z)^2+(x^2+y^2)}} \quad (4)$$

$$\left|\frac{x'}{x}\right|=\left|\frac{y'}{y}\right|=\frac{|\overline{QT}|}{\sqrt{x^2+y^2}}=\frac{f+z-|\overline{QM}|}{f+z} \quad (5)$$

$$R^2=(R\sin\chi-x')^2+y'^2+(|\overline{QM}|-z+R\cos\chi)^2 \quad (6)$$

From solving the above system of Eqs. (4)–(6), the depth of absorption, Z_a, in the sample when the laser is focused at an arbitrary position, $P_0(x_0,y_0,z_0)$, on the surface of the ball/pin can be obtained, as follows:

$$Z_a(x,y,z)=\frac{\sqrt{(f+z)^2+(x^2+y^2)}}{f+z}\times\left\{-\left[2R\sin\chi\left(\frac{x}{f+z}\right)-2(z-R\cos\chi)-2\left(\frac{x^2+y^2}{f+z}\right)\right]\right.$$
$$\left.+\sqrt{\left[2R\sin\chi\left(\frac{x}{f+z}\right)-2(z-R\cos\chi)-2\left(\frac{x^2+y^2}{f+z}\right)\right]^2-4\left[1+\frac{x^2+y^2}{(f+z)^2}\right]\times(x^2+y^2+z^2-2xR(\sin\chi+\cos\chi))}\right\}\times\left\{2\left[1+\frac{x^2+y^2}{(f+z)^2}\right]\right\}^{-1} \quad (7)$$

where R is the radius of the ball, and χ is the polar angle from the focal position to the top of the ball as shown in Fig. 2. When $x,y,z<<f$, Eq. (7) can be greatly simplified to become:

$$Z_a(x,y,z)\approx-\frac{Rx}{f}\sin\chi+z-R\cos\chi$$
$$+\sqrt{(R\cos\chi)^2+2xR(\sin\chi+\cos\chi)+2zR\cos\chi-(x^2+y^2)} \quad (8)$$

In this study, we selected $x_0=y_0=0$, and translate into the spherical coordinate system shown in Fig. 2(a). Accordingly, Eq. (1) becomes:

$$I_{obs}(z_0)\propto\iiint_V I(\omega)G(x,x_0,y,y_0,z,z_0)dxdydz$$

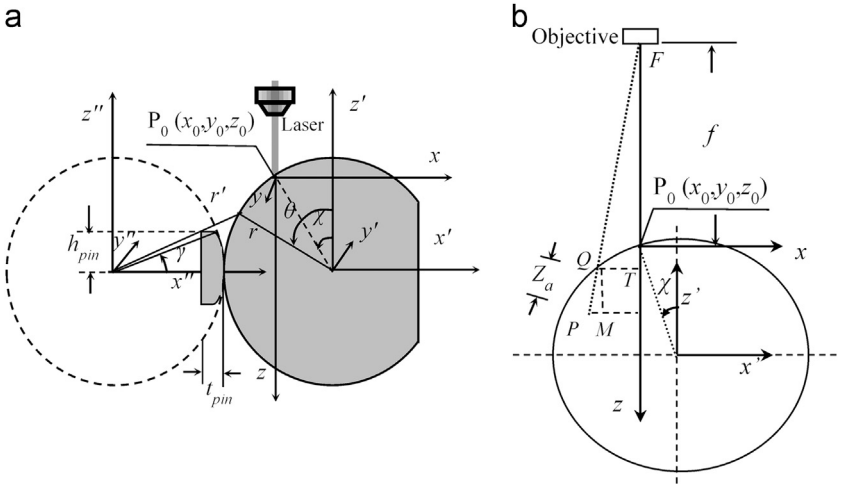

Fig. 2 – (a) Schematic drafts of the sliding contact, choice of Cartesian and spherical coordinate systems for the pin-on-ball geometry, and (b) collection at the objective lens of the fluorescence emission from an arbitrary point within the laser probe.

$$= \int_{r=0}^{R}\int_{\theta=0}^{\pi}\int_{\varphi=0}^{2\pi} I(\omega) \times \exp\left\{-2\frac{\left[r\sin\theta + R\sin\chi\cos\varphi()^2 + (R\sin\chi\sin\varphi)^2\right]}{\left[(R\cos\chi - r\cos\theta - z_0)\times\tan\left(\arcsin\left(\frac{NA}{n}\right)\right)\right]^2 + B_0^2}\right\} \times \frac{p^2}{p^2 + (R\cos\chi - r\cos\theta - z_0)^2}\left\{\exp\left[-2\alpha_{eff}Z_a(r,\theta,\varphi)\right]\right\} \times \left[1 - \frac{f + R\cos\chi - r\cos\theta}{\sqrt{(f + R\cos\chi - r\cos\theta)^2 + \left(\frac{D}{2}\right)^2}}\right] r^2\sin\theta\, dr\, d\theta\, d\varphi + \int_{r'=R-t_{pin}}^{R}\int_{\theta'=\frac{\pi}{2}-\gamma}^{\frac{\pi}{2}+\gamma}\int_{\varphi'=-\gamma}^{\gamma} I(\omega) \times \exp\left\{-2\frac{\left[(r'\sin\theta' + (R\sin\chi - 2R)\cos\varphi')^2 + ((R\sin\chi - 2R)\sin\varphi')^2\right]}{\left[(R\cos\chi - r'\cos\theta - z_0)\times\tan\left(\arcsin\left(\frac{NA}{n}\right)\right)\right]^2 + B_0^2}\right\} \times \frac{p^2}{p^2 + (R\cos\chi - r'\cos\theta - z_0)^2}\left\{\exp\left[-2\alpha_{eff}Z_a(r',\theta',\varphi')\right]\right\} \times \left[1 - \frac{f + R\cos\chi - r'\cos\theta'}{\sqrt{(f + R\cos\chi - r'\cos\theta')^2 + \left(\frac{D}{2}\right)^2}}\right] r'^2\sin\theta'\, dr'\, d\theta'\, d\varphi' \quad (9)$$

where, $\gamma = \arcsin(h_{pin}/R)$, with h_{pin} and t_{pin} being the height (2.5 mm) and the thickness (5.35 mm) of the pin, respectively.

3.2. *In situ analysis of local temperature at the contact point*

During wear test, part of the kinetic energy is converted into frictional heat, which develops and propagates from the contact zone. This eventually results in high temperature at the contact between pin and ball. A thermal analysis of the temperature gradient at the contact point should then be based on the solution of a heat-propagation equation from a hot-spot source of appropriate shape (i.e., frictional heat generation from the contact zone and transfer through the bulk in the absence of lubricant). Heat transfer can be described by a partial differential equation, which locates the distribution of heat (or variation in temperature) in a given region over time. The temperature function, $T(x,y,z,t)$, thus depends on the three spatial variables, (x,y,z), and the time variable, t. Heat conduction in a stationary medium is described by:

$$\frac{\partial^2 T}{\partial x^2} + \frac{\partial^2 T}{\partial y^2} + \frac{\partial^2 T}{\partial z^2} = \frac{1}{\alpha}\frac{\partial T}{\partial t} \quad (10)$$

where α is the thermal diffusivity of the material. In the case of an instantaneous point source, the heat, Q, developed at $t=0$ at the point (x_0, y_0, z_0) of the sample, is a delta function, which will cause a temperature distribution in the sample, as follows:

$$T(x,y,z,t) = \frac{Q}{\rho c_p\sqrt{(4\pi\alpha t)^3}}\exp\left[\frac{(x-x_0)^2 + (y-y_0)^2 + (z-z_0)^2}{4\alpha t}\right] \quad (11)$$

where ρ denotes the material density and c_p its specific heat. In the case of a time dependent point source, the effect of heat inputs at different times is directly additive since heat is not a vectorial quantity. Therefore, the temperature distribution at any time can be set as just the integration over time of a series of instantaneous heat sources:

$$T(x,y,z,t) = \int_0^t \frac{Q}{\rho c_p\sqrt{(4\pi\alpha t')^3}}\exp\left[\frac{(x-x_0)^2 + (y-y_0)^2 + (z-z_0)^2}{4\alpha t'}\right] dt' \quad (12)$$

In the case of the rotating femoral head, the contact time can be considered as $t = d_c/v$, with v being the rotation speed of the head, and d_c the diameter of the trajectory along which the contact occurs with the pin. Thermal diffusivity and density values of the investigated materials are listed in Table 1.

It has been reported that the widths of the chromophoric fluorescence bands R_1 and R_2 of Al_2O_3 obey a linear dependence on temperature (0.108 and 0.077 $cm^{-1}/^{\circ}C$, respectively (Ma and Clarke, 1994)). Therefore, temperature variations at the contact point can be monitored *in situ* from detecting the broadening of fluorescence bands during wear testing. Note that bandwidth can also be affected by stress gradients, but such broadening is negligible in comparison with that arising from temperature increases (Ma et al., 1994). The measured temperature variation at the focal point taken as the origin of the Cartesian axes (x_0,y_0,z_0), can be then expressed through the PRF formalism, according to the following equation:

$$\overline{\Delta T}(t) = \frac{\iiint_{V_{pin}} G(x,y,z)\times\Delta T_{pin}(x,y,z,t)dxdydz + \iiint_{V_{ball}} G(x,y,z)\times\Delta T_{ball}(x,y,z,t)dxdydz}{\iiint_{V_{pin}+V_{ball}} G(x,y,z)dxdydz} \quad (13)$$

where $\overline{\Delta T}(t)$ is the temperature difference sensed by the fluorescence probe and thus averaged over its finite volume, and ΔT_{pin} and ΔT_{ball} are the real temperature changes at the contact point on the pin and the head side of the contact, respectively.

3.3. *Stress evaluation by in situ fluorescence spectroscopy*

During wear test in the tribometer, two stress components are generated at the contact point between pin and ball: a shear stress generated by friction, and a uniaxial pressure created by the two parts in contact under load. The shear stress can be considered to be constant in the contact area, while the uniaxial pressure applied at the contact between pin and ball in turn generates two variable stress components, which can be given as (Huber, 1904; Deeg, 1992):

$$\sigma_{zz}(x) = \frac{8aE'}{\pi R}\left\{(1+\upsilon)\left[\frac{x}{a}\operatorname{arccot}\left(\frac{x}{a}\right) - 1\right] + \frac{a^2}{2(a^2+x^2)}\right\} \quad (14)$$

Table 1 – Parameters involved with temperature, thermal fields, contact stress and stress distribution calculations.

	E (GPa)	υ	α (mm^2/s)	ρ (g/cm^3)	P (N)	Vr (mm/s)	d_{ball} (mm)
Delta	350	0.22	7.63	4.25	10	100	32
Forte	380	0.23	10.5	4.0	10	100	32

$$\sigma_{xx}(x) = \frac{8aE'}{\pi R}\frac{a^2}{a^2+x^2} \tag{15}$$

where the radius of the contact area on the pin, a, is given by:

$$a = \sqrt[3]{\frac{3PR}{4E'}} \tag{16}$$

with P being the contact load, and E' and R are given by:

$$E' = \left(\frac{1-\upsilon_1^2}{E_1} + \frac{1-\upsilon_2^2}{E_2}\right)^{-1} \tag{17}$$

$$R = \left(\frac{1}{R_1} + \frac{1}{R_2}\right)^{-1} \tag{18}$$

with υ and E being the Poisson's ratio and the Young's modulus, respectively, of the pin and of the ball (subscripts 1 and 2, respectively). R_1 and R_2 are the radii of curvature of the pin and of the ball, respectively. In self-mating sliding couples, $E_1=E_2$ and $\upsilon_1=\upsilon_2$, and in the selected geometry, $R_1=R_2$. Values of these parameters are listed in Table 1. However, because the applied load is perpendicular to the stem that holds the ball, also a moment is generated on the ball, and the contact area can be different from the ideal one. Moreover, any damage on the ball in the simulation process can result in a change in the contact radius. According to these considerations, in the present computational approach, we shall take $d_c=2a$, but treat the contact radius, a, as an unknown parameter.

The stress field stored on the surface around the contact point can again be determined by using fluorescence piezo-spectroscopy, taking advantage of the characteristic R_1 and R_2 fluorescence bands produced by Cr^{3+} impurities in Al_2O_3. In the case of untextured polycrystalline samples, the observed spectral shift of a selected fluorescence line will depend on the magnitude (or, in the general case, on the trace) of the applied stress tensor (Ma and Clarke, 1994) (i.e., thus including the effects of both frictional and pressure forces), as follows:

$$\Delta\omega = \frac{1}{3}\Pi_{ii}\sigma_{ii} \tag{19}$$

where $\prod_{ii}/3$ is an average piezo-spectroscopic (PS) coefficient over all the possible crystallographic directions, and is a material property. The average PS coefficient of the R_1 fluorescence band was experimentally determined by a preliminary calibration procedure as $-2.53\ cm^{-1}$/GPa and $-3.0\ cm^{-1}$/GPa, for *delta* and *forte* materials, respectively. According to the above PRF formalism, the measured spectroscopic band shifts, $\Delta\omega$, at the (focal) contact point, arising from local stress distributions developed in both pin and head ball, can be expressed by the following equation:

$$\overline{\Delta\omega}(t) = \frac{\iiint_{V_{pin}} G(x,y,z)\times\Delta\omega_{pin}(x,y,z,t)dxdydz + \iiint_{V_{ball}} G(x,y,z)\times\Delta\omega_{ball}(x,y,z,t)dxdydz}{\iiint_{V_{pin}+V_{ball}} G(x,y,z)dxdydz} \tag{20}$$

where $\overline{\Delta\omega}(t)$ is the frequency shift sensed by the fluorescence probe and thus averaged over its finite volume, and $\Delta\omega_{pin}$ and $\Delta\omega_{ball}$ are the real frequency shifts at the contact point on the pin and the head side of the contact, respectively.

4. Results and discussion

4.1. *Determination of probe response functions for composite and monolithic sliding couples*

The first step needed to unfold property gradients within the volume of a laser probe focused at the contact point is represented by the experimental determination of the PRF that characterizes the interaction between the incoming laser and the pin-on-ball system. To properly derive the probe parameters, defocusing of the laser along the sample depth was carried out at different locations of the femoral head by gradually shifting the laser focal plane along the direction of the incoming light, with concurrently recording the intensity variations of the corresponding fluorescence spectra at each focal position. Fig. 3 shows the probe-defocusing behavior for the R_1 band under a 100× objective lens, namely a plot of normalized spectral intensity at the contact point of the sliding couple ($\chi=90^\circ$) as a function of focal position z_0. For comparison, the results of defocusing experiments conducted at the top location of the femoral head ($\chi=0^\circ$) are also shown. Although both Al_2O_3 and ZrO_2 are inherently anisotropic materials, their small grain sizes enable

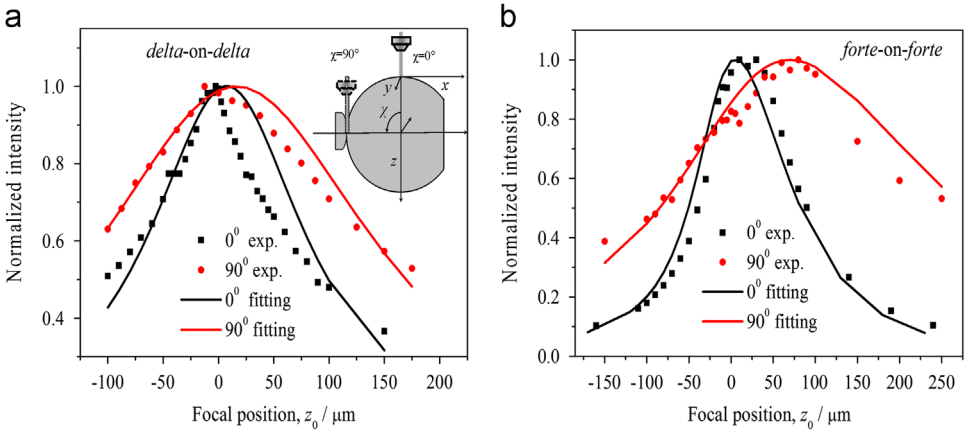

Fig. 3 – Experimental plots of normalized intensity of the R_1 band vs. defocus distance, z_0, as collected at different locations of (a) *delta*-on-*delta* and (b) *forte*-on-*forte* sliding couples, respectively. The χ angles of the plots are given in inset of (a). The corresponding least-square fitting curves were calculated according to Eq. (9).

averaging polarization effects, thus making light scatter similar to the case of isotropic materials. PRF collected for *delta*-on-*delta* and *forte*-on-*forte* couples could always be fitted using Eq. (9) as a trial function, with the best fits also plotted in Fig. 3. The best fitting curve for the *delta* material at $\chi=0^\circ$ gives $p=84\,\mu m$ and $\alpha=0.066\,\mu m^{-1}$ while at $\chi=90^\circ$ the parameter p equals 175 μm. In the case of the *forte* material, at $\chi=0^\circ$ the parameters p and α are equal to 47 μm and $0.012\,\mu m^{-1}$, respectively, while at $\chi=90^\circ$ $p=130\,\mu m$. The difference in the numerical values of the p parameter at the position $\chi=90^\circ$as compared to $\chi=0^\circ$ arises from the peculiarity of the laser/sample interaction in this geometry. The waist of the laser spot was estimated as about 1 μm in the focal plane on the top of the ball ($\chi=0^\circ$), but it is strongly altered at the contact point. In fact, part of the laser cone focused at $\chi=90^\circ$ encountered the surface of the femoral ball before reaching the focal position. Note that the effect of the refractive index, n, is to bend light rays towards the normal to the surface. Consequently, within the material, z_0 is increased by a factor of n with respect to its value in free space. In other words, the refraction of the light through the ceramic material increases the effective spot size at the focal plane.

4.2. *Measurements of local temperature at contact point by fluorescence spectroscopy*

As mentioned above, temperature variations can be determined from the variation of time-dependent fluorescence spectra *in situ* recorded at the contact point during running a wear test on the ceramic couples. Fig. 4(a) shows the variation of contact temperature, ΔT, as obtained from broadening of the R_1 fluorescence band. Data are plotted as a function of sliding distance for *delta*-on-*delta* and *forte*-on-*forte* sliding couples, respectively. Because of laser probe broadening, the measured values only show average temperatures. Since a quite steep gradient is expected to reduce temperature away from the contact point, the measured (average) temperature can be significantly lower than the true temperature. With the knowledge of thermal diffusivity for the investigated materials, best fitting to the experimental data was carried out according to Eqs. (12) and (13). Accordingly, the real temperature values at the center of the contact area between ball and pin could be calculated for both materials, as shown in Fig. 4(b). The convoluted curves corresponding to the plots in Fig. 4(b) are the full lines plotted in Fig. 4(a). A rapid increase and then a saturation of the local temperature at the contact point were commonly found, due to friction between the sliding components. A lower contact temperature was found in the *forte*-on-*forte* sliding couple as compared to the *delta*-on-*delta* one, which is the consequence of the lower friction coefficient in the former couple (i.e., 0.41 vs. 0.52 (Puppulin et al., in press)).

The steep temperature gradient generated (at regime) during sliding in the neighborhood of the contact point from the pin side can also be plotted according to Eq. (12), as shown in Fig. 5. The plots show similar trends but quite different temperature ranges, consistent with the plots in Fig. 4. A similar estimation of the temperature gradient was also attempted from the ball side. However, unlike the pin that was subjected to a continuous frictional load, the time needed for the ball to complete one-round rotation at the

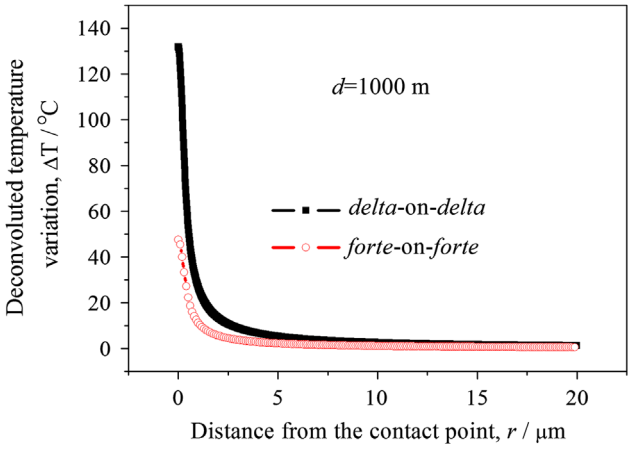

Fig. 5 – Comparison between gradients of deconvoluted regime temperature as a function of distance from the contact point along the radial direction, r, as recorded for *delta*-on-*delta* and *forte*-on-*forte* sliding couples.

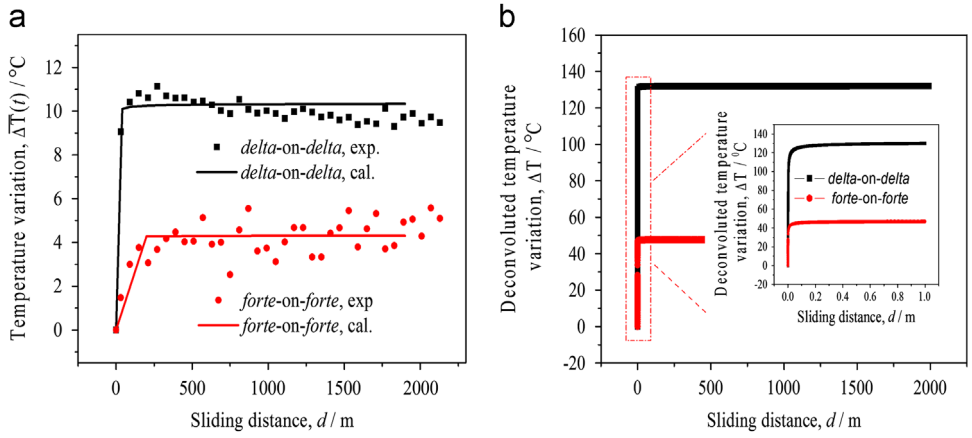

Fig. 4 – Variation of (a) measured temperature and (b) real temperature as a function of sliding distance at the contact point between pin and ball for *delta*-on-*delta* and *forte*-on-*forte* sliding couples. The convoluted best fitting curves were calculated according to Eq. (13). Enlargements of the transient zones to regime are shown for better clarity in inset of (b).

speed selected in this study, namely $t_1 = d_{ball}/vr = 0.32$ s, was by far longer than the time needed for heat diffusion away from the contact point from the ball side. Therefore, only insignificant changes in temperature (<1 °C) could be detected on the ball surface.

4.3. *Stress assessments in situ at the contact point*

From fluorescence spectra recorded *in situ* at the contact point as a function of sliding distance, contact stress magnitudes could also be retrieved. However, in this case, one complication arises from fluorescence band shift being equally affected by stress and temperature (McCumber and Sturge, 1963). Shift of the R1 band with temperature was reported as $-0.144\ cm^{-1}/°C$ (He and Clarke, 1995). Therefore, an additional computational step was needed, according to which the spectral shift components arising from stress and temperature could be separated (i.e., spectral shifts computed from the known temperature field at each sliding distance were preliminary subtracted from the observed shifts). Fig. 6 shows the variation of the observed spectral shifts of the R_1 band at the contact point (i.e., with respect to its initial spectral position at the beginning of the test) as a function of sliding distance. Also in this case *delta*-on-*delta* and *forte*-on-*forte* sliding couples were compared and the raw data directly obtained from the measurements only corresponded to average shifts weighted through the PRF over the probe volume. Convoluted best-fitting curves are shown in Fig. 6, which corresponded to the deconvoluted plots at the contact location between pin and ball surfaces shown in Fig. 7. The recursive best-fitting routine was performed according to Eqs. (14)–(20), with the constant parameters used for the calculations in the case of the two different materials as listed in Table 1. Accordingly, the actual magnitudes of the stress field around the contact point could be retrieved. Fig. 7(a) shows the deconvoluted stress variation at the contact point as a function of sliding distance for the case of *delta*-on-*delta* and *forte*-on-*forte* sliding couples. Rather high compressive stresses were found at the contact point, which gradually decreased in magnitude with increasing sliding distance. This finding can be ascribed to the generation of scars on both ball and pin, with consequent increase of the contact area between the sliding counterparts. On the other hand, the stress magnitude at sliding regime rapidly decreased with increasing distance away from the contact point towards the center of the ball (or pin) (cf. Fig. 7(b)). A significantly lower stress magnitude was found for the *forte*-on-*forte* sliding couple as compared to the *delta*-on-*delta* one. A similar difference in maximum contact forces was also recorded by the bi-axial load cell of the tribometer (Puppulin et al., in press). Such large difference in stress magnitude might again be related to the higher friction coefficient of the *delta*-on-*delta* sliding couple. However, also contributions related to polymorphic transformation in the zirconia phase, which was found in the *delta* material by spectroscopic analyses of the scars at the end of the test, cannot be ruled out. The stress results, complementing the temperature assessments in the previous section, show that the composite couple behaves in a more "dissipative" way as compared to the monolithic one. This is, however, a very intriguing task, if one

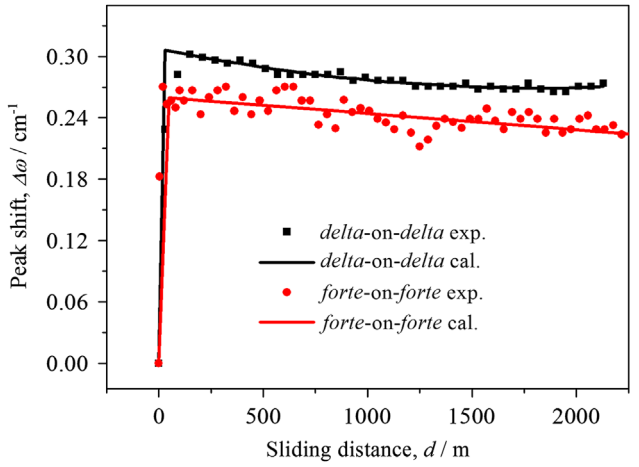

Fig. 6 – Variation of the observed spectral shifts of the R_1 band as a function of sliding distance when the laser was focused at the contact point for *delta*-on-*delta* and *forte*-on-*forte* sliding couples. The corresponding best fitting curves were calculated according to Eqs. (14)–(20).

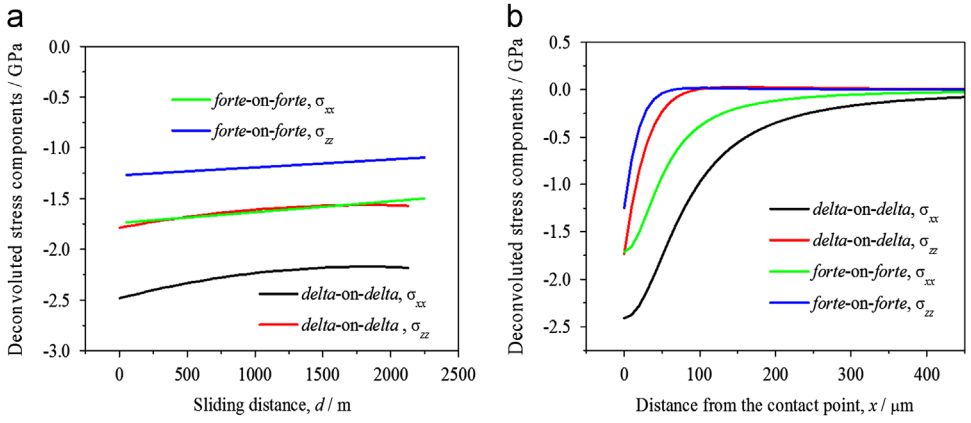

Fig. 7 – Variation of deconvoluted contact stress magnitudes, which were detected at the contact points for *delta*-on-*delta* and *forte*-on-*forte* sliding couples as a function of: (a) sliding distance; and, (b) radial direction from the center of the pin at sliding regime.

considers that the composite couple was also found to experience at least a three-fold lower specific wear rate as compared to the monolithic one (3.67×10^{-14} m^2/N vs. 9.67×10^{-14} m^2/N at the ball side, and 2.23×10^{-17} m^2/N vs. 1.02×10^{-16} m^2/N on the pin side (Puppulin et al., in press)).

5. Conclusions

In situ assessments of contact stress and local temperature at the contact point were carried out in a specially designed pin-on-ball tribometer during dry sliding of ceramic-on-ceramic femoral heads by means of fluorescence microprobe spectroscopy. Experimental investigations on two commercially available ceramic-on-ceramic couples BIOLOX®*delta* and BIOLOX®*forte* could be performed with taking advantage of the intense fluorescence emission of Cr^{3+} impurities contained in Al_2O_3. The sample-probe interaction at the contact point was elucidated with experimentally obtaining the PRFs for the two materials through a defocusing procedure, so that a deconvolutive computational routine could be set up to remove averaging effects inside the probe volume. Accordingly, true variations of local temperature and stress at the contact point could be retrieved from the observed time-dependent broadening and shift of a selected spectral band. Both materials showed a high magnitude of compressive stress at the contact point, but lower stress magnitudes could be found in the monolithic couple. In addition, a significantly higher temperature, in the order of 134 °C, was found at the contact point of the composite couple in dry conditions obtained as a consequence of its higher friction coefficient in the particular configuration of the wear test selected here. Despite the more "dissipative" behavior of the composite sliding couple as compared to the monolithic one, the composite couple showed a significantly higher wear resistance than the monolithic one, which proves the effectiveness in hip joint applications of its synergistically improved microstructure.

REFERENCES

Atkinson, A., Jain, S.C., 1999. Spatially resolved stress analysis using Raman spectroscopy. Journal of Raman Spectroscopy 30, 885–891.

Cherif, K., Gueroult, B., Rigaud, M., 1997. Al_2O_3–ZrO_2 debris life cycle during wear: effects of the third body on wear and friction. Wear 208, 161–168.

Deeg, E.W., 1992. New algorithms for calculating Hertzian stresses, deformations, and contact zone parameters. AMP Journal of Technology 2, 14–24.

Goldsmith, A.A., Dowson, D., 1999. A multi-station hip joint simulator study of the performance of 22 mm diameter zirconia-ultra-high molecular weight polyethylene total replacement hip joints. Proceedings of the Institution of Mechanical Engineers, Part H: Journal of Engineering in Medicine 213, 77–90.

He, J., Clarke, D.R., 1995. Determination of the piezospectroscopic coefficients for chromium-doped sapphire. Journal of the American Ceramic Society 78, 1347–1353.

Huber, M.T., 1904. Zur Theorie der Berührung fester elastischer Körper. Annals of Physics 14, 153–163.

Joly-Pottuz, L., Martin, J.M., Belin, M., Dassanoy, F., 2007. Sudy of inorganic fullerenes and carbon nanotubes by *in situ* Raman tribometry. Applied Physics Letters 91, 153107 1-3.

Kerkwijk, B., Winnubst, A.J.A., Verweij, H., Metselaar, H.S.C., Mulder, E.J., Schipper, D.J., 1999. Tribological properties of nanoscale alumina–zirconia composites. Wear 225–229, 1293–1302.

Korres, S., Dienwiebel, M., 2010. Design and construction of a novel tribometer with online topography and wear measurement. Review of Scientific Instruments 81, 063904 1-7.

Lipkin, D.M., Clarke, D.R., 1995. Sample-probe interactions: sampling microscopic property gradients. Journal of Applied Physics 77, 1855–1863.

Ma, Q., Clarke, D.R., 1994. Piezospectroscopic determination of residual stresses in polycrystalline alumina. Journal of the American Ceramic Society 77, 298–302.

Ma, Q., Pompe, W., French, J.D., Clarke, D.R., 1994. Residual-stresses in Al_2O_3–ZrO_2 composites—a test of stochastic stress models. Acta Metallurgica et Materialia 42, 1673–1681.

McCumber, D.E., Sturge, M.D., 1963. Linewidth and temperature shift of the *R* lines in ruby. Journal of Applied Physics 34, 1682–1684.

McKellop, H.A., D'Lima, D., 2008. How have wear testing and joint simulator studies helped to discriminate among materials and designs?. Journal of the American Academy of Orthopaedic Surgeons 16, S111–S119.

Nair, R.P., Griffin, D., Randall, N.X., 2009. The use of the pin-on-disk tribology test method to study three unique industrial applications. Wear 267, 823–827.

Patton, S., Zabinski, J.S., 2002. Advanced tribometer for *in situ* studies of friction, wear, and contact condition—advanced tribometer for friction and wear studies. Tribology Letters 13, 263–273.

Piconi, C., Maccauro, G., Muratori, F., Brach del Prever, E., 2003. Alumina and zirconia ceramics in joint replacements. Journal of Applied Biomaterials and Biomechanics 1, 19–32.

Puppulin, L., Leto, A., Zhu, W., Sugano, N., Pezzotti, G., 2012. Innovative tribometer for *in situ* spectroscopic analyses of wear mechanisms and phase transformation in ceramic femoral heads. Journal of the Mechanical Behavior of Biomedical Materials http://dx.doi.org/10.1016/j.jmbbm.2013.12.004, in press.

Ramamurti, B.S., Estok, D.M., Jasty, M., Harris, W.H., 1998. Analysis of the kinematics of different hip simulators used to study wear of candidate materials for the articulation of total hip arthroplasties. Journal of Orthopaedic Research 16, 365–369.

Saikko, V., 2005. A 12-station anatomic hip joint simulator. Proceedings of the Institution of Mechanical Engineers, Part H: Journal of Engineering in Medicine 219, 437–448.

Zemzemi, F., Bensalem, W., Rech, J., Dogui, A., Kapsa, P., 2008. New tribometer designed for the characterization of the friction properties at the tool/chip/workpiece interface in machining. Tribotest 14, 11–25.

Zhu, W., Pezzotti, G., 2005. Spatially resolved stress analysis in Al_2O_3/3Y-TZP multilayered composite using confocal fluorescence spectroscopy. Applied Spectroscopy 59, 1042–1048.